American Mineralogist, Volume 81, pages 595–602, 1996

A synchrotron radiation, HRTEM, X-ray powder diffraction, and Raman spectroscopic study of malayaite, $CaSnSiO_5$

LEE A. GROAT,[1] STEFAN KEK,[2] ULRICH BISMAYER,[3] CLAUDIA SCHMIDT,[4] HANS GEORG KRANE,[5] HINRICH MEYER,[3] LEONA NISTOR,[6] AND GUSTAAF VAN TENDELOO[6]

[1]Department of Geological Sciences, University of British Columbia, Vancouver, British Columbia V6T 1Z4, Canada
[2]FR Kristallographie, Universität des Saarlandes, D-66041 Saarbrücken, Germany
[3]Mineralogisch-Petrographisches Institut, Universität Hamburg, D-20146 Hamburg, Germany
[4]Institut für Mineralogie, Universität, Welfengarten 1, D-30060 Hanover, Germany
[5]Institut für Kristallographie, Universität, Kaiserstrasse 12, D-76128 Karlsruhe, Germany
[6]Universiteit Antwerpen (RUCA), Groenenborgerlaan 171, B-2020 Antwerp, Belgium

ABSTRACT

Synchrotron radiation, high-resolution transmission electron microscopy (HRTEM), X-ray powder diffraction, and Raman spectroscopy were used to study the structure and thermal behavior of malayaite, $CaSnSiO_5$. No indications of deviation from $A2/a$ symmetry and no structural transitions were observed between 100 and 870 K. HRTEM revealed that the material is free of domains and antiphase boundaries. However, the lattice constants, cell volume, and Raman-active phonons show a thermal discontinuity near 500 K, which is possibly related to variation of the coordination sphere around the highly anisotropic Ca position.

INTRODUCTION

Malayaite, $CaSnSiO_5$, is a rare mineral found in skarn deposits. The structure of malayaite was solved by Higgins and Ribbe (1977) in space group $A2/a$ and was refined to $R = 4.7\%$ from data collected with conventional Zr-filtered Mo radiation. They showed that the structure consists of corner-sharing SnO_6 polyhedra that form chains parallel to a. These are linked to sevenfold-coordinated Ca atoms by SiO_4 tetrahedra. Malayaite is isostructural with titanite, $CaTiSiO_5$. Takenouchi (1971) showed that there is complete solid solution between the two phases at elevated temperatures. The solvus is asymmetric, with a maximum of 888 ± 15 K at a composition of $Ti_{0.75}Sn_{0.25}$.

Synthetic titanite undergoes an antiferrodistortive transition at 496 K from a monoclinic high-temperature phase ($A2/a$) to a monoclinic low-temperature phase ($P2_1/a$). As described by Taylor and Brown (1976) and Ghose et al. (1991), the transformation in titanite involves displacement of the Ti atoms from the centers of the TiO_6 octahedra parallel to the a (relatively large shift), b, and c axes (both relatively small shifts). This displacement pattern leads to antiparallel sublattices of octahedral chains because within individual chains the Ti atoms shift in the same direction. This transition in synthetic titanite has been studied in great detail because of the antiferroelectric distortion pattern (Taylor and Brown 1976; Zhang et al. 1995), the nonclassical critical behavior (Ghose et al. 1991; Bismayer et al. 1992), the mobile antiphase boundaries above T_c (Van Heurck et al. 1991), the pseudo-spin characteristics (Bismayer et al. 1992), and the corresponding effective critical exponent of the order parameter (Salje et al. 1993a). In perfect agreement with observations by Zhang et al. (1995), Kek et al. (1994) recently showed that in synthetic titanite between 850 and 496 K the Ca atoms are displaced parallel to a and c, so that the true symmetry of the intermediate regime is $P2_1/n$. However, the average symmetry is $A2/a$ because of antiphase domains.

The situation in natural titanite is more complex. Higgins and Ribbe (1976) found that in natural samples, both Al^{3+} and Fe^{3+} substitute for Ti. At levels of substitution greater than approximately 5 mol% (Al + Fe) titanite shows diffuse $k + l = 2n + 1$ reflections, which disappear at approximately 15–20 mol% (Al + Fe). Higgins and Ribbe (1976) suggested that octahedral sites containing Al or Fe serve as boundaries on either side of domains of Ti octahedra with atoms displaced in opposite directions. The greater the amount of substitution, the more abundant are the domains, which results in more diffuse $k + l = 2n + 1$ reflections.

In their study of the malayaite structure Higgins and Ribbe (1977) found no evidence of violating reflections, even on very-long-exposure precession photographs. They suggested that the formation of domains leading to an average $A2/a$ symmetry in titanite is dependent on the substitution of cations smaller than Ti. They proposed that because Sn is approximately 0.085 Å larger than Ti it is more likely to occupy the center of the octahedra; therefore, the symmetry of malayaite is more likely to be $A2/a$. No information on the thermal behavior of the malayaite structure and related physical properties was available.

This study was undertaken to determine whether (1)

0003–004X/96/0506–0595$05.00

TABLE 1. Crystallographic data and refinement information for malayaite

a (Å)	7.1535(6)	Crystal size (mm)	0.19 × 0.11 × 0.06
b (Å)	8.8933(8)	Wavelength (Å)/mono	0.5597(1)/Si(111)
c (Å)	6.6674(6)	Reflections collected	4017
β (°)	113.342(7)	Unique data (2/m)	1384
V (Å^3)	389.50	Unobserved ($\|F_o\| < 3\sigma$)	13
Space group	$A2/a$	R (%)	1.51
Z	4	R_w (%)	2.31

there are reflections violating extinction conditions for $A2/a$ that are too weak or diffuse to be seen on precession photographs; (2) the apparent $A2/a$ symmetry is the result of a domain structure; and (3) the thermal development of the structure or its metric shows any discontinuities.

SAMPLE

The samples used in this study are from a skarn approximately 4 km north of Ash Mountain, near McDame, in northern British Columbia, Canada. Electron microprobe analyses were performed with a Cameca Camebax instrument, operating at 20 kV and 25 nA. The following standards were used: Al_2O_3 (Al), quartz (Si), wollastonite (Ca), Fe_2O_3 (Fe), and SnO_2 (Sn). Wavelength scans were used to search for additional elements; none were detected. The results were processed with the Cameca PAP program. They show 21.82 wt% SiO_2, 21.06 wt% CaO, 0.17 wt% Fe_2O_3, and 56.86 wt% SnO_2 (average of eight analyses), corresponding to 0.98 Si, 1.01 Ca, 0.01 Fe, and 1.01 Sn atoms per formula unit (renormalized on the basis of five anions). Hence, the malayaite is almost pure $CaSnSiO_5$, with a negligible amount of Fe substituting for Sn.

SINGLE-CRYSTAL X-RAY DIFFRACTOMETRY

Single-crystal X-ray diffraction data were collected at 295 K with the four-circle diffractometer at HASYLAB beam line D3 during dedicated experiments (4.5 GeV) of Doris III. The wavelength used throughout the experiment was 0.5597(1) Å. The sample showed sharp Bragg reflections with full-width at half-maximum (FWHM) values (0.012–0.016°, ω scan) typical of good quality mosaic crystals. The lattice parameters, refined from 16 centered reflections, are a = 7.1535(6), b = 8.8933(8), c = 6.6674(6) Å, β = 113.342(7)°. A continuous scan mode was used where the ω axis was rotated at a constant speed throughout the Bragg position, with scalers recorded and cleared at fixed time intervals. The scan speed was adjusted to record (after insertion of appropriate attenuator combinations) a maximum of 2500 counts, without exceeding measurement times of 0.1–1.0 s/step. A total of 4017 reflections (including test reflections) were recorded comprising two asymmetric units with $(\sin\theta)/\lambda \leq 0.947$ Å^{-1}.

The A-centered lattice was confirmed by measuring 243 unique reflections with $k + l = 2n + 1$; none were observed at $F^2 < 3\sigma_{F^2}$. Reflection scans at liquid-nitrogen temperature also showed no significant intensity even for counting times of 3.5 s/step.

Data reduction included normalization to the primary beam intensity monitor and an on-line correction for the (measured) beam polarization, following the procedure of Kirfel and Eichhorn (1990). The data were corrected for absorption by approximating the shape of the crystal with a polyhedron (eight faces). The unique data set (R_{int} = 2.9%) comprised 1384 reflections (13 with $|F| < 3\sigma_{|F|}$).

With no evidence to suggest violation of the A centering, the structure was refined in space group $A2/a$. Starting values for positional and thermal parameters were taken from Higgins and Ribbe (1977). Least-squares refinements were based on $|F|$ with weights = $[\sigma_F^2 + (0.02 \cdot F)^2]^{-1}$, chosen to minimize variation of mean $\omega\Delta^2$ as functions of F_o and $(\sin\theta)/\lambda$. An isotropic extinction correction (Becker and Coppens 1974a, 1974b) was applied using a type-1 Lorentzian distribution. The refined parameter was $g = 0.61(2) \times 10^4$; the most strongly affected reflections were $\bar{2}11$ (y = 0.45), 220 (0.59), and 020 (0.73), where y is the intensity reduction relative to the kinematic value. Scattering factors for the neutral atoms were taken from the *International Tables for X-ray Crystallography,* volume 4 (Ibers and Hamilton 1974). Anomalous dispersion corrections were taken from Cromer and Liberman (1970). Computer programs used in the refinements include modified versions of ORFLS (Busing et al. 1962), ORFFE (Busing et al. 1964), and ORTEP (Johnson 1965).

Refinement with anisotropic displacement factors for all atoms led to convergence at R = 1.7% (R_w = 2.8%). Attempts to split the strongly anisotropic Ca site were unsuccessful because the positions converged and the R values increased dramatically. Refinement with anharmonic displacement parameters (i.e., higher cumulants up to third order, "g tensor") for the Ca site led to a large decrease in R_w. Only one tensor element (c_{112}) was significant; refinement with this additional parameter led to a reduction of R_w from 2.8 to 2.3%. Crystallographic data and refinement information are given in Table 1, final atom parameters in Table 2, selected interatomic distances and angles in Table 3, detailed data collection and processing information in Table 4, details of the refinement results (including g-tensor elements for Ca) in Table 5, and observed and calculated structure factors in Table 6.[1]

[1] A copy of Tables 4–6 may be ordered as Document AM-96-612 from the Business Office, Mineralogical Society of America, 1015 Eighteenth Street NW, Suite 601, Washington, DC 20036, U.S.A. Please remit $5.00 in advance for the microfiche.

TABLE 2. Final atom parameters for malayaite

	x	y	z	U_{eq}	U_{11}	U_{22}	U_{33}	U_{12}	U_{13}	U_{23}
Si	¾	0.68196(4)	½	685(12)	409(8)	420(10)	476(7)	0	151(5)	0
Sn	½	½	0	663(8)	362(6)	417(6)	494(5)	−18(1)	143(4)	4(4)
Ca	¼	0.66262(4)	½	1289(4)	3240(10)	486(8)	753(7)	0	−129(6)	0
O1	¾	0.58681(4)	0	944(8)	540(10)	570(10)	1340(10)	0	470(9)	0
O2	0.91140(13)	0.56776(3)	0.67552(4)	883(8)	956(9)	797(10)	561(8)	298(7)	154(6)	154(6)
O3	0.37224(4)	0.71195(3)	0.89032(4)	895(8)	910(10)	600(10)	758(9)	252(6)	414(7)	72(6)

Note: U_{ij} values have been multiplied by 10^5.

The refined structure is as described by Higgins and Ribbe (1977). However, details are presented here because of the increased precision in values obtained using synchrotron radiation. As shown in Figures 1 and 2, the malayaite structure consists of corner-sharing $[SnO_3]^{6-}$ chains that extend parallel to a and are further linked along their lengths by SiO_4 tetrahedra to form type-I $[Sn(SiO_4)O_3]^{6-}$ chains (Moore 1970). The tetrahedral vertices not linked to the central octahedral chain cross-link to adjacent chains to form a mixed tetrahedral-octahedral framework. Within this framework are large cavities containing Ca atoms in irregular sevenfold-coordinated polyhedra.

The most remarkable feature of the malayaite structure is the extreme anisotropy of the Ca position. Because none of the other atoms show this degree of distortion it is not likely the result of an error in the absorption correction. The anisotropy of the Ca position may represent true thermal vibration or it may be due to antiphase domains. The irregular coordination sphere around the Ca atom (Fig. 1) suggests the former because the thermal vibration of the Ca atom is largely constrained by Ca-O bonds to be parallel to a. However, the study by Kek et al. (1994) of the structure of synthetic titanite at 100, 295, and 530 K suggests that the anisotropy may be related to antiphase domains previously observed by Van Heurck et al. (1991). They found that the thermal parameters of the Ca position were strongly anisotropic at all three temperatures and were able to refine a split Ca position at 530 K [Ca-Ca distance of 0.17(5) Å]. If the strong anisotropy of the Ca position is due to antiphase domains the apparent $A2/a$ symmetry of malayaite may be an average symmetry similar to that seen by Kek et al. (1994) in synthetic titanite above 496 K. To answer this question we decided to use transmission electron microscopy (TEM) to look for antiphase boundaries (APBs). X-ray powder diffraction (XRD) and Raman spectroscopy were used to study the response of the structure to heating.

TABLE 3. Selected interatomic distances (Å) and angles (°) in malayaite

Si-O2	× 2	1.6320(3)	O2-Si-O2[b]		103.03(3)
Si-O3[g]	× 2	1.6421(4)	O2-Si-O3[a]	× 2	112.86(1)
⟨Si-O⟩		1.6371	O2b-Si-O3[a]	× 2	109.07(1)
			O3a-Si-O3[g]		109.86(3)
Sn-O1	× 2	1.9479(1)	⟨O-Si-O⟩		109.46
Sn-O2[b]	× 2	2.0878(2)			
Sn-O3[c]	× 2	2.0961(3)	O1-Sn-O2[b]	× 2	89.07(1)
⟨Sn-O⟩		2.0439	O1-Sn-O2[h]	× 2	90.93(1)
			O1-Sn-O3[c]	× 2	85.24(1)
Ca-O1[d]		2.2284(5)	O1-Sn-O3[e]	× 2	94.76(1)
Ca-O2[e]	× 2	2.4145(4)	O2b-Sn-O3[c]	× 2	90.76(1)
Ca-O3[f]	× 2	2.4344(2)	O2b-Sn-O3[e]	× 2	89.24(1)
Ca-O3[a]	× 2	2.7415(3)	⟨O-Sn-O⟩		90.00
⟨Ca-O⟩		2.4870			

Note: a = 1 − x, 1 − y + ½, 1 − z + ½; b = ½ − x + 1, y, 1 − z; c = x, y, − 1 + z; d = ¼, 1 − y + ½, ½; e = 1 − x, 1 − y, 1 − z; f = ½ − x, y, 1 − z; g = ½ + x, 1 − y + ½, −1 + z + ½; and h = ½ + x − 1, 1 − y, −1 + z.

TRANSMISSION ELECTRON MICROSCOPY

Samples for transmission electron microscopy were prepared by crushing the crystallites and suspending the fragments on copper grids covered with a holey carbon film. A double-tilt heating holder was used for the in situ electron diffraction experiments in a Philips CM 20 electron microscope. High-resolution transmission electron microscopy (HRTEM) was performed at room temperature in a JEOL 4000EX microscope.

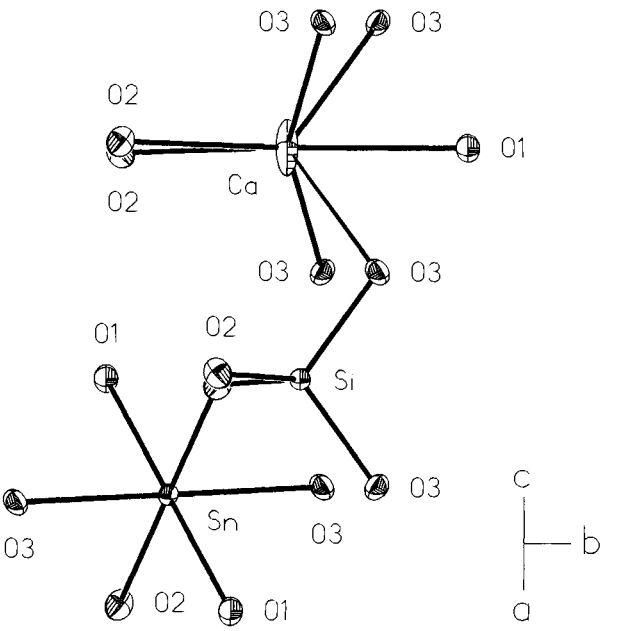

FIGURE 1. ORTEP plot of the characteristic structural units in malayaite (99% probability ellipsoids).

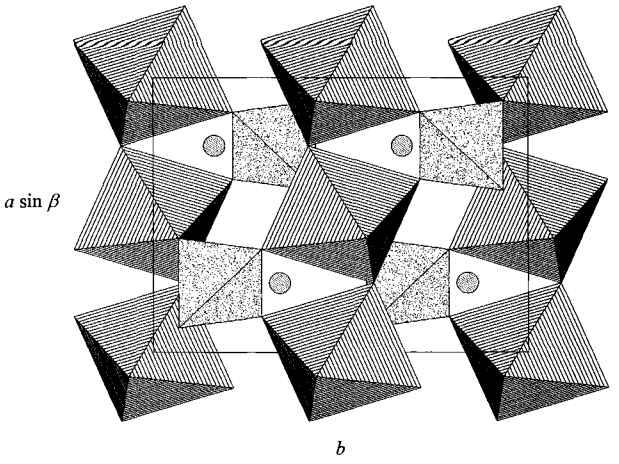

FIGURE 2. Polyhedral representation of the malayaite structure, projected onto (001).

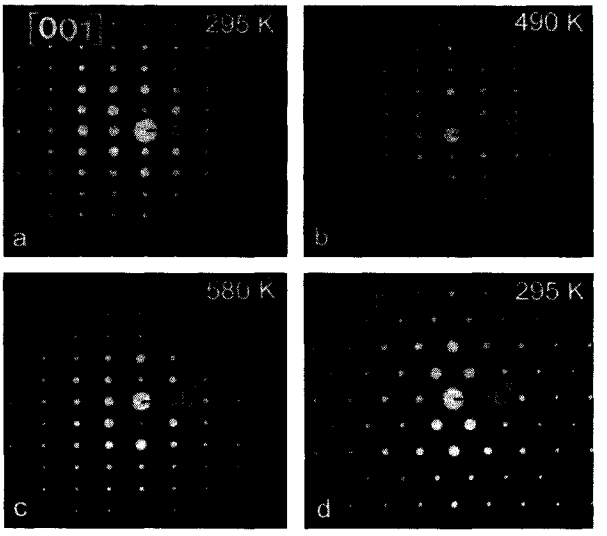

FIGURE 3. Selected-area diffraction (SAD) patterns along the (a) [001] zone at room temperature (295 K); (b) [001] zone at ~490 K; (c) [001] zone at ~580 K; (d) [101] zone at room temperature.

Some results of the TEM study are shown in Figure 3. Figures 3a and 3d show selected-area diffraction (SAD) patterns along the [001] and [101] zones at room temperature (295 K). All the diffraction spots are sharp and round, and only those corresponding to $k + l = 2n$ are present. This shows that the symmetry is $A2/a$ at room temperature. Figures 3b and 3c depict SAD patterns along the [001] zone near 490 and 580 K. There is little apparent difference between the patterns recorded at room temperature and 490 K. The only modification seen in the pattern recorded at 580 K is broadening of the diffraction spots because of increased Debye-Waller factors. Patterns recorded between 580 and approximately 870 K show no structural changes. Apparently no phase transition occurs from room temperature to 870 K. At all temperatures the sample was observed to be stable under the electron beam.

Unlike in titanite, $CaTiSiO_5$ (Van Heurck et al. 1991), no superstructure reflections were observed in the room-temperature [001] and [101] zones. Consequently, no domain boundaries are expected in real-space images. Neither low magnification nor high-resolution observations showed any evidence for such domain formation, not even on a nanometer or subnanometer scale.

X-RAY POWDER DIFFRACTOMETRY

In preparation for X-ray powder diffractometry the sample was crushed, ground to a fine powder, and mixed with Si as an internal standard. The powder was spread over a platinum heating element in an evacuated heating cell equipped with Kapton windows. The furnace was mounted on a diffractometer with a monochromatic CuK_1 X-ray beam (incident diameter 0.1 × 10 mm) and an INEL 4 K-PSD detector. The temperature was monitored with ultra-thin thermocouples (Pt-Rh alloy) welded to the heating element. Quartz and langbeinite $[K_2Cd_2(SO_4)_3]$ were used as temperature calibration standards. Experimental details are given in Salje et al. (1993b).

Lattice parameters were refined using the LCLSQ 8.4 program (Burnham 1991). The results are shown in Figure 4. The graphs of a, b, and c vs. temperature show slight changes in slope at approximately 473 K. This is much less apparent in the graph of β vs. temperature because of scatter in the data. However, the graph of cell volume vs. temperature shows a distinct break in slope at approximately 493 K. Extrapolation of the high-temperature curve gives a volume of approximately 388.3 Å^3 at 300 K as opposed to an apparent volume of 389 Å^3 for the low-temperature curve extrapolated to the same temperature.

Because no APBs were seen in the HRTEM experiment it is unlikely that the XRD results indicate a structural phase transition. It is more likely that they represent a slight readjustment of the average structure with increasing temperature; this may primarily involve the volume of the coordination sphere around the highly anisotropic Ca position with its largest anisotropic displacement parameter U_{11} (Table 5).

RAMAN SPECTROSCOPY

Raman spectroscopic measurements were performed with a spectrometer consisting of a 4W argon laser light source (λ = 488 nm) with continuously variable polarization directions. The beam was doubly focused on a sample mounted in a furnace. The light scattered at 90° to the sample was focused on the entrance slit of a double monochromator and detected by a Peltier-cooled photomultiplier attached to a phonon counter. The fit proce-

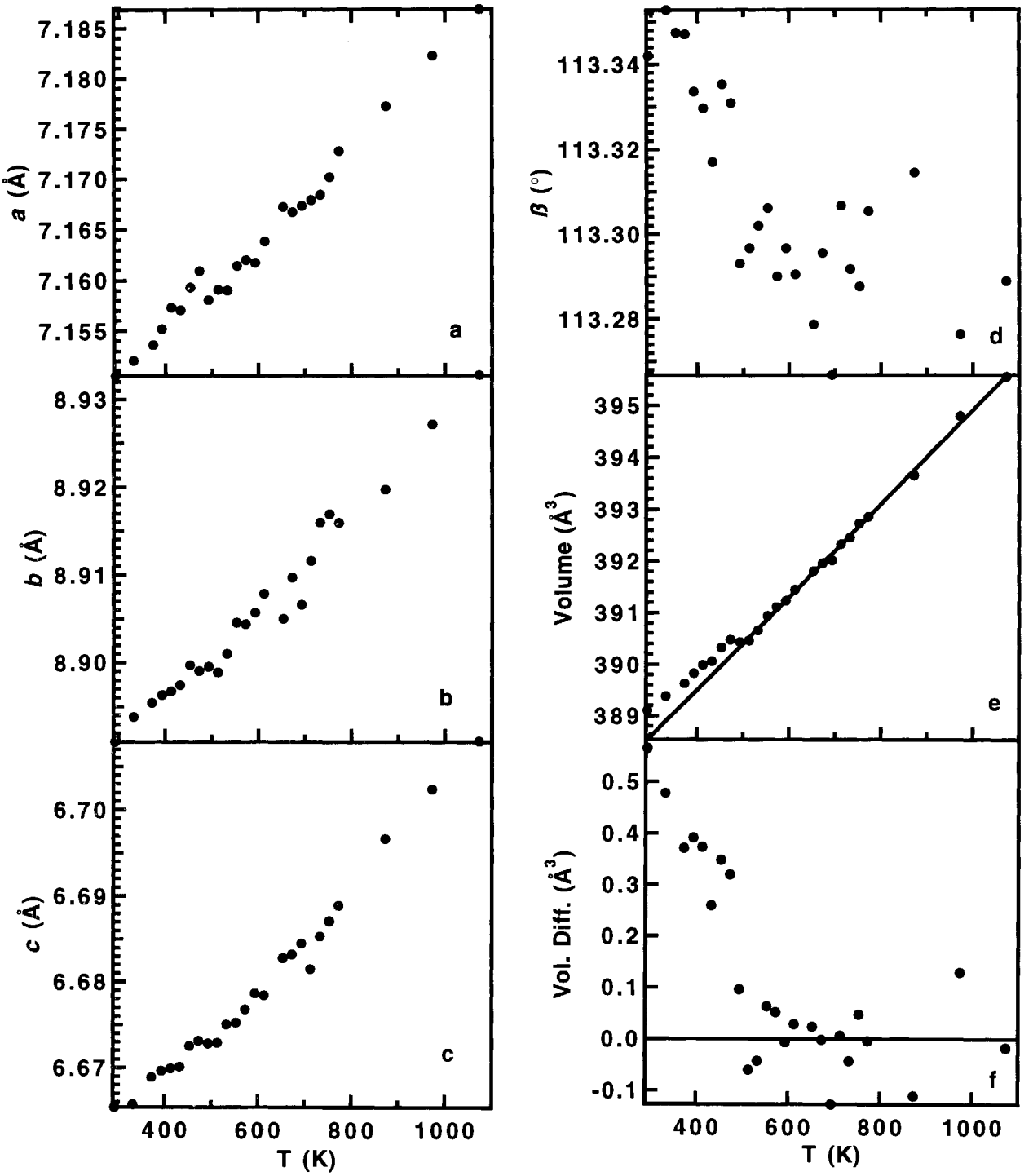

FIGURE 4. Temperature dependence of (a) a, (b) b, (c) c, (d) β, and (e) cell volume. (f) Difference of linearly extrapolated high-temperature data and measured volume.

dure described in Bismayer et al. (1986) was used for line-profile analysis.

The $A2/a$ phonon spectrum (A_g symmetry) of malayaite at 300 K is shown in Figure 5, and A_g Raman spectra between 470 and 620 cm^{-1} collected at temperatures between 300 and 953 K are shown in Figure 6. The optically active representations are $\Gamma_{tot} = 9A_g + 12B_g + 11A_u + 13B_u$ and $\Gamma_{acoust} = A_u + 2B_u$. Twenty-one active modes

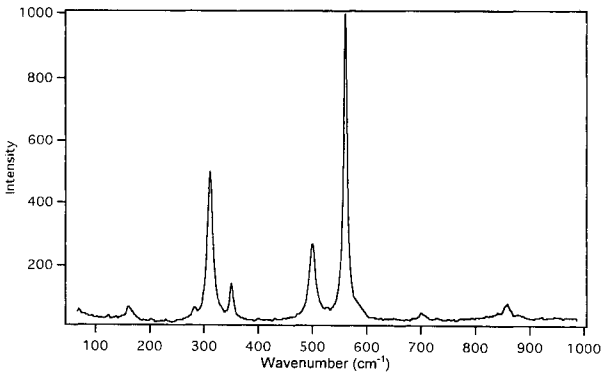

FIGURE 5. A_g Raman spectrum of malayaite at 300 K.

TABLE 7. Frequencies (cm^{-1}) of the most prominent Raman signals of malayaite at 110 K

Frequencies	Intensities	Frequencies	Intensities
75	w	328	w
109	s	340	vs
142	s	412	w
176	vs	450	w
197	w	510	w
227	w	520	s
250	s	595	vs
280	s	802	vw
295	w	837	s
305	s	895	vw

Note: Error is ± 1 cm^{-1}, intensities are scaled, vw, w, s, and vs in increasing strength.

are expected in the first-order Raman spectrum. The frequencies of the most intense bands are given in Table 7. The line widths of all phonons are approximately 10 cm^{-1} at room temperature. At 0 K the FWHM of the mode near 560 cm^{-1} extrapolates to approximately 4 cm^{-1} (Fig. 7a), which indicates that there is practically no broadening of the density of states owing to disorder phenomena or perturbation of the translational symmetry. On heating, the frequency of the mode near 560 K (Fig. 7b) decreases by approximately 5 cm^{-1} from 300 to 800 K. Coupling between the volume change and the optical A_g phonon leads to the change of slope of the phonon frequency near 500 K.

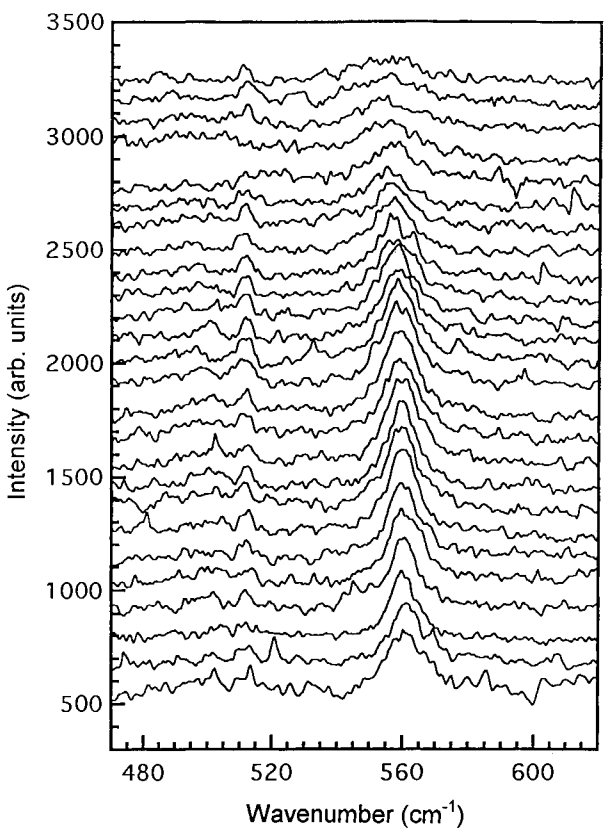

FIGURE 6. A_g Raman spectra between 470 and 620 cm^{-1} collected at the following temperatures (bottom to top; in K): 300, 385, 397, 453, 473, 483, 513, 523, 533, 543, 553, 563, 583, 603, 623, 643, 663, 683, 713, 743, 773, 803, 833, 873, 913, 953.

DISCUSSION

The evolution of lattice parameters at high temperatures shows a change in slope at approximately 500 K, but this does not seem to correspond to the same symmetry-breaking process seen in synthetic titanite. In malayaite the thermal change in slope of the lattice parameters and the volume is probably due to an anomaly involving the highly anisotropic Ca position. In the case of a true phase transition the excess volume is proportional to the square of the order parameter of the system, which displays the thermodynamic anharmonicity. In fact, the difference between the measured and the extrapolated volume (Fig. 4f) decreases progressively as temperature approaches 500 K. If a thermally controlled collapse of the coordination sphere around the Ca site is the mechanism responsible for the measured changes, the overall volume couples with this local effect, which reflects the thermal evolution of the structure without leading to a change of the global symmetry. We state that in this sense the excess volume cannot be correlated with a classical order parameter but with the triggering distortion such as found in langbeinite (Percival 1990). Further work is underway to characterize this event. The integrated intensities (Fig. 7c) obtained from the Raman spectra (Fig. 6) show that the macroscopic volume change is compatible with the weak anharmonicity of the structure on a local length scale.

Our work has shown that there is no evidence of domain structure in malayaite. Therefore, the *A2/a* symmetry must reflect that the large Sn atoms are already at the centers of the octahedral sites and are not displaced, as are the Ti atoms in primitive titanite. As suggested by Higgins and Ribbe (1977), it would be interesting to ex-

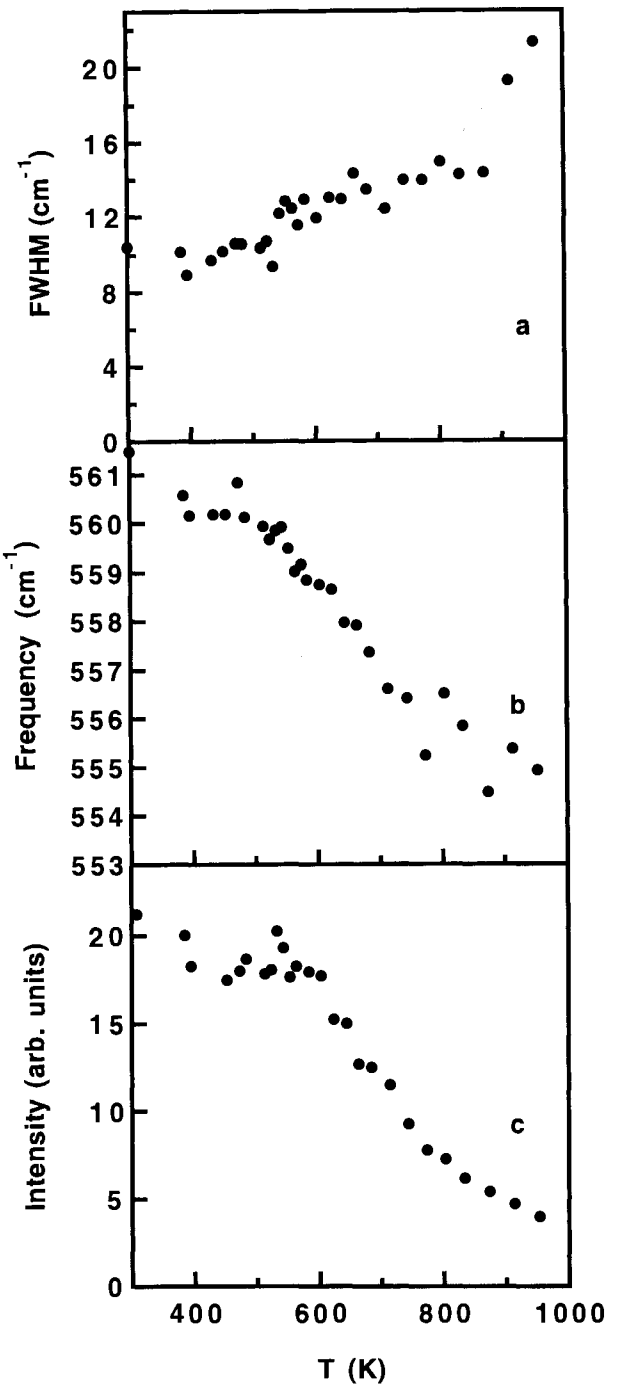

FIGURE 7. (a) FWHM of the 560 cm^{-1} A_g mode as a function of temperature (error ±1.5 cm^{-1}). (b) Frequency of the 560 cm^{-1} mode as a function of temperature (error ±1 cm^{-1}). (c) Integrated intensity of the 560 cm^{-1} mode as a function of temperature (error ±10%).

amine single crystals of titanite containing small amounts of Sn or other cations larger than Ti to see what effect these would have on domain formation and thus the overall symmetry.

ACKNOWLEDGMENTS

The authors thank B.S. Wilson for providing the samples and acknowledge the technical assistance of A. Graeme-Barber, G. Adiwidjaja, and K.H. Klaska. The authors also thank T.S. Ercit for his constructive comments. The research was supported by grants from the National Science and Engineering Research Council (Canada) to L.A.G. and from the Deutsche Forschungsgemeinschaft and the Bundesminister für Forschung und Technologie to S.K., C.S., H.M., and U.B.

REFERENCES CITED

Becker, P., and Coppens, P. (1974a) Extinction within the limit of validity of the Darwin transfer equations: I. General formalisms for primary and secondary extinction and their application to spherical crystals. Acta Crystallographica, A30, 129–147.

——— (1974b) Extinction within the limit of validity of the Darwin transfer equations: II. Refinement of extinction in spherical crystals of SrF_2 and LiF. Acta Crystallographica, A30, 148–153.

Bismayer, U., Salje, E.K.H., Jansen, N., and Dreher, S. (1986) Raman scattering near the structural phase transition of As_2O_5: Order parameter treatment. Journal of Physics, C19, 4537–4545.

Bismayer, U., Schmal, W., Schmidt, C., and Groat, L.A. (1992) Linear birefringence and X-ray diffraction studies on the structural phase transition in titanite, $CaTiSiO_5$. Physics and Chemistry of Minerals, 18, 260–266.

Burnham, C.W. (1991) LCLSQ version 8.4. Least-squares refinement of crystallographic lattice parameters. Harvard University, Cambridge, Massachusetts.

Busing, W.R., Martin, K.O., and Levy, H.A. (1962) ORFLS: A FORTRAN crystallographic least-squares program. Oak Ridge National Laboratory, Report ORNL-TM-305.

——— (1964) ORFFE: A FORTRAN crystallographic function and error program. Oak Ridge National Laboratory, Report ORNL-TM-305.

Cromer, D.T., and Liberman, D.A. (1970) Relativistic calculation of anomalous scattering factors for X-rays. Journal of Chemical Physics, 53, 1891–1898.

Ghose, S., Ito, Y., and Hatch, D.M. (1991) Paraelectric-antiferroelectric phase transitions in titanite, $CaTiSiO_5$: I. A high temperature X-ray diffraction study of the order parameter and transition mechanism. Physics and Chemistry of Minerals, 17, 604–610.

Higgins, J.B., and Ribbe, P.H. (1976) The crystal chemistry and space groups of natural and synthetic titanites. American Mineralogist, 61, 878–888.

——— (1977) The structure of malayaite, $CaSnOSiO_4$, a tin analog of titanite. American Mineralogist, 62, 801–806.

Ibers, J.A., and Hamilton, W.C., Eds. (1974) International tables for X-ray crystallography, vol. 4, 366 p. Kynoch, Birmingham, U.K.

Johnson, C.K. (1965) A FORTRAN thermal-ellipsoid plot program for crystal structure illustrations. Oak Ridge National Laboratory, Report ORNL-3794.

Kek, S., Aroyo, M., Bismayer, U., Meyer, H., Schmidt, C., Eichhorn, K., and Krane, H.G. (1994) Synchrotron radiation study of the crystal structure of titanite ($CaTiSiO_5$) at 100 K, 295 K and 530 K: Model for a two step structural transition. HASYLAB/DESY, Annual Report, p. 453–454.

Kirfel, A., and Eichhorn, K. (1990) Accurate structure analysis with synchrotron radiation: The electron density in Al_2O_3 and Cu_2O. Acta Crystallographica, A46, 271–284.

Moore, P.B. (1970) Structural hierarchies among minerals containing octahedrally coordinating oxygen: I. Stereoisomerism among corner-sharing octahedral and tetrahedral chains. Neues Jahrbuch für Mineralogie Monatshefte, 163–173.

Percival, M.J.L. (1990) A trigger mechanism in an improper ferroelastic: The langbeinite structure. In E.K.H. Salje, Ed., Phase transitions in ferroelastic and co-elastic crystals, p. 296. Cambridge University Press, Cambridge.

Salje, E.K.H., Schmidt, C., and Bismayer, U. (1993a) Structural phase transitions in titanite, $CaTiSiO_5$: A Raman spectroscopic study. Physics and Chemistry of Minerals, 19, 502–506.

Salje, E.K.H., Graeme-Barber, A., Carpenter, M.A., and Bismayer, U. (1993b) Lattice parameters, spontaneous strain and phase transitions in $Pb_3(PO_4)_2$. Acta Crystallographica, B49, 387–392.

Takenouchi, S. (1971) Hydrothermal synthesis and consideration of the genesis of malayaite. Mineral Deposita, 6, 335–347.

Taylor, M., and Brown, G.E. (1976) High-temperature structural study of the $P2_1/a \rightleftharpoons A2/a$ phase transition in synthetic titanite, $CaTiSiO_5$. American Mineralogist, 61, 435–447.

Van Heurck, C., Van Tendeloo, G., Ghose, S., and Amelinckx, S. (1991) Paraelectric-antiferroelectric phase transitions in titanite, $CaTiSiO_5$: II. Electron diffraction and electron microscopic studies of transition dynamics. Physics and Chemistry of Minerals, 17, 604–610.

Zhang, M., Salje, E.K.H., Bismayer, U., Unruh, H.G., Wruck, B., and Schmidt, C. (1995) Phase transition(s) in titanite $CaTiSiO_5$: An infrared spectroscopic, dielectric response and heat capacity study. Physics and Chemistry of Minerals, 22, 41–49.

Manuscript received June 20, 1995
Manuscript accepted December 29, 1995